PHYSICAL REVIEW B **79**, 184102 (2009)

First-principles determination of crystal structures, phase stability, and reaction thermodynamics in the Li-Mg-Al-H hydrogen storage system

A. R. Akbarzadeh,[1] C. Wolverton,[2] and V. Ozolins[1]

[1]*Department of Materials Science and Engineering, University of California, P.O. Box 951595, Los Angeles, California 90095-1595, USA*

[2]*Department of Materials Science and Engineering, Northwestern University, Evanston, Illinois 60208, USA*

(Received 5 December 2008; revised manuscript received 23 March 2009; published 5 May 2009)

First-principles density-functional theory (DFT) calculations have been used to investigate the crystal structures, thermodynamic stability, and decomposition pathways of Li-Mg-Al-H hydrogen storage compounds. We find that the recently discovered $LiMg(AlH_4)_3$ compound is stable with respect to solid-state decomposition into $LiAlH_4$ and $Mg(AlH_4)_2$; however, we also find that $LiMg(AlH_4)_3$ is unstable with respect to hydrogen release and decomposes exothermically into $LiMgAlH_6$, Al, and H_2 with a calculated $T=300$ K enthalpy of -7.3 kJ/(mol H_2), in excellent agreement with the weakly exothermic value of -5 kJ/(mol H_2) obtained from differential scanning calorimetry measurements [M. Mamatha *et al.*, J. Alloys Compd. **407**, 78 (2006)]. $LiMgAlH_6$ is a stable intermediate, which has two competing endothermic decomposition pathways for H_2 release: one going directly into the binary hydrides of Li and Mg and the other proceeding via the formation of an intermediate Li_3AlH_6 phase, with room-temperature enthalpies of +18.6 and +16.6 kJ/(mol H_2), respectively. Using database searching based on known crystal structures from the inorganic crystal structure database, we predict that the hypothetical $MgAlH_5$ compound should assume the orthorhombic $BaGaF_5$ prototype structure, in contrast to a previous DFT study of $MgAlH_5$, [A. Klaveness *et al.*, Phys. Rev. B **73**, 094122 (2006)]. However, the decomposition enthalpy of $MgAlH_5$ is only weakly endothermic, +1.1 kJ/(mol H_2), and therefore this compound is not expected to occur in the high-temperature decomposition sequence of Mg alanate. We also present a comprehensive investigation of the phonon spectra and vibrational thermodynamics of Li-Mg-Al-H compounds, finding that vibrations typically decrease reaction enthalpies by up to 10 kJ/mol H_2 at ambient temperatures and significantly lower reaction entropies.

DOI: 10.1103/PhysRevB.79.184102 PACS number(s): 64.70.Hz, 68.43.Bc, 82.60.Cx, 84.60.−h

I. INTRODUCTION

Introduction of environmentally clean hydrogen-powered vehicles is crucially dependent on finding a material that could store hydrogen at high gravimetric and volumetric densities and could reversibly release and absorb hydrogen at moderate temperatures and pressures. This is a difficult task since it requires combining a multitude of physical, chemical, thermodynamic, and kinetic factors in one materials system. Because of their high hydrogen content and attractive storage densities, several solid-state storage materials based on complex hydrides (alanates, borohydrides, and amides) have emerged as promising candidates for use in on-board storage systems.[1] Ti-doped $NaAlH_4$ is the most studied material from this class, exhibiting a storage density of $\sim$4.5 wt % H_2 and reasonably good thermodynamics and kinetics.[2] However, even though the reversible storage capacity of $NaAlH_4$ is roughly twice as high as that of conventional metal hydrides, it still falls significantly below the system targets for on-board automotive applications.

Hence, much recent work has focused on alanates with higher capacities than $NaAlH_4$, such as the lithium and magnesium alanate systems. However, both of these systems exhibit substantial drawbacks. Although $LiAlH_4$ has a higher gravimetric density of hydrogen than $NaAlH_4$, it is unsuitable for on-board storage due to poor thermodynamics: it decomposes exothermically into Li_3AlH_6, Al, and H_2 and cannot be rehydrided at practical pressures.[1] The hexahydride Li_3AlH_6 has better thermodynamic properties than $LiAlH_4$, favoring hydrogen release near ambient temperatures, but it has only a modest H_2 storage capacity and exhibits very poor kinetics, releasing hydrogen at significant rates only at 220–270 °C.[3] Similarly, $Mg(AlH_4)_2$ has a high theoretical capacity of $\sim$9 wt % H_2, but it also suffers from poor thermodynamics. It has nearly zero enthalpy of reaction when decomposing into MgH_2, Al, and H_2, and thus its thermodynamic stability is far below the desired range for reversible hydrogen storage systems.[4]

In view of the limitations of the various simple alanates, considerable effort has gone into searching for *mixed* alanate compounds with an optimal combination of thermodynamic and kinetic properties. We address one such mixed alanate system here based on the Li-Mg-Al-H system. Bialkalimetallic alanates, such as $LiNa_2AlH_6$, have been investigated as possible candidates for light-weight hydrogen storage systems (see, e.g., Refs. 1 and 5–8 and references therein). Recently, the crystal structures of two mixed Li-Mg alanates $LiMgAlH_6$ and $LiMg(AlH_4)_3$ were established experimentally.[5,6] These findings are interesting because the compound represents the only known mixed-cation alanate tetrahydride and $LiMgAlH_6$ is the only known alanate hexahydride compound with mixed-valence cations (Li^+ and Mg^{2+}). In this paper, we report a comprehensive density-functional theory (DFT) study of the phase stability, thermodynamic properties, vibrational spectra, and crystal structures of the various Li-Mg alanate compounds, including all known compounds [$LiAlH_4$, Li_3AlH_6, $LiMg(AlH_4)_3$ $LiMgAlH_6$, and $Mg(AlH_4)_2$], as well as theoretical predictions for the yet-undiscovered $MgAlH_5$. We also report on

TABLE I. List of compounds with their space groups and the calculated $T=0$ K formation enthalpies ΔH_f, experimental formation enthalpies $\Delta H_f^{\text{Exp.}}$, ZPE, vibrational energies $H_{\text{vib}}^{300\ \text{K}}$ (all in kJ/mol), and entropies $S_{\text{vib}}^{300\ \text{K}}$ (in J/mol K) at $T=300$ K. The last column provides the information on supercell sizes used for our frozen phonon calculations.

Compound	Space group	ΔH_f	ΔH_f other DFT	$\Delta H_f^{\text{Exp.}}$	ZPE	$H_{\text{vib}}^{300\ \text{K}}$	$S_{\text{vib}}^{300\ \text{K}}$	Phonon supercell
H_2		0			25.9	25.9	0.	$1\times1\times1$
Li	$Im\bar{3}m$ (229)	0			3.9	8.2	27.4	$2\times2\times2$
Mg	$P63/mmc$ (194)	0			2.9	7.9	31.9	$2\times2\times1$
Al	$Fm\bar{3}m$ (225)	0			3.6	8.0	25.4	$4\times4\times4$
LiH	$Fm\bar{3}m$ (225)	−83.9	−87.0[a]		21.9	25.4	19.7	$4\times4\times4$
MgH_2	$P42/mmm$ (136)	−62.8	−64.0[a]	−73.1[b]	39.1	44.6	31.9	$3\times3\times4$
$LiAlH_4$ [c]	$P121/c1$	−102.6	−111[d]	−107[e],−107.2[f]	80.7	92.7	71.1	$2\times1\times1$
Li_3AlH_6 [g]	$R\bar{3}$ (148)	−295.5	−308.4[d]	−298.47[e],−311.1[f]	129.5	146.4	91.9	$1\times1\times1$
$LiMgAlH_6$ [h]	$P321$ (150)	−184.8			126.5	140.5	77.3	$1\times1\times2$
$LiMg(AlH_4)_3$ [i]	$P2_1/c$ (14)	−192.6			237.6	271.6	206.8	$1\times1\times1$
$Mg(AlH_4)_2$ [j]	$P\bar{3}m_1$ (164)	−62.0			154.4	178.3	152.7	$2\times2\times2$
$MgAlH_5$ ($BaGaF_5$-type)	$P2_12_12_1$ (19)	−73.8			102.9	113.8	62.5	$1\times2\times2$

[a]Reference 13.
[b]Reference 26.
[c]Reference 29.
[d]Reference 8.
[e]Reference 30.
[f]Reference 31.
[g]Reference 32.
[h]Reference 6.
[i]Reference 5.
[j]Reference 33.

preferred reaction pathways and reaction thermodynamics in the Li-Mg-Al-H system.

II. METHODS

We used first-principles DFT calculations with the generalized gradient approximation (GGA) of Perdew and Wang (PW91).[9] Electron-ion interactions were treated within the projected augmented wave (PAW) approach,[10] as implemented in the Vienna *ab initio* simulation package (VASP).[11] The basis set for the electronic wave functions was defined by a plane-wave cutoff energy of 875 eV. The Brillouin zones of solid phases were sampled using $4\times4\times4$ Monkhorst-Pack k-point meshes.[12] Structural relaxations of atomic positions, cell shapes, and cell volumes were carried out until the residual forces were less than 0.01 eV/Å and stresses were less than 0.1 GPa. The energy of the H_2 molecule was calculated by placing it in a cubic box with a side length of 10 Å. The frozen phonon dynamical matrix method was used to determine the normal-mode frequencies of ionic vibrations within the harmonic approximation; the technical details of these calculations are the same as in Ref. 13. Table I gives the information on supercells that were used in phonon calculations. The phonon density-of-states (PDOS) curves were obtained by adding normalized Gaussians of 25 cm^{-1} width centered at the directly calculated normal-mode frequencies, and the vibrational entropies and enthalpies were obtained by summing over the normal modes of supercells. Atom-decomposed partial vibrational entropies were obtained by summing the entropy contributions of all phonon modes with weights given by the atomic component in the mode eigenvector,

$$S_i = \sum_s |\mathbf{e}_i(s)|^2 S_{\text{harm}}\left(\frac{\hbar\omega_s}{2k_BT}\right), \tag{1}$$

where index i runs over the atoms in the unit cell, index s runs over phonon modes with frequencies ω_s, $\mathbf{e}_i(s)$ is the component of atom i in the normalized mode eigenvector, and $S_{\text{harm}}(x)=x/\tanh(x)-\ln[2\sinh(x)]$ is the harmonic phonon entropy function. An analogous definition was adopted to obtain partial atom-decomposed vibrational enthalpies and partial phonon densities of states.

III. CRYSTAL STRUCTURES

Hydrogen storage reactions in multicomponent complex hydrides can be complicated and often follow unexpected pathways. It is therefore difficult to simply guess the preferred thermodynamic pathway from chemical intuition alone. We have developed a computational tool [the grand canonical linear programming method (GCLP) (Ref. 14)] that bypasses these difficulties by the automated detection of thermodynamically favored reactions. We used this method initially to uncover preferred decomposition reactions in the Li-Mg-N-H system.[14] Subsequently, we[15,16] and others[17] have demonstrated the utility of this method by applying it to a wide variety of hydrogen storage systems.

However, the GCLP method requires, as a first step, the identification of the set of possible compounds in a given multicomponent system that can participate in hydrogen storage reactions. In the Li-Mg-Al-H system, we include in our set the well-known compounds Li, Mg, Al, LiH, MgH_2, AlH_3, $LiAlH_4$, Li_3AlH_6, and $Mg(AlH_4)_2$ (see Table I). We exclude some phases, such as intermetallics in the Al-Li and

TABLE II. Calculated DFT energies of prototype structures that were used in the crystal structure database searching for $LiMgAlH_6$.

Prototype structure	Pearson symbol	Energy (kJ/mol)
$NaCaAlF_6$	hP27	0
$LiCaAlF_6$	hP18	7.7
$NaCaAlF_6$	mP72	7.7
$LiSmAlF_6$	hP18	32.7
$NaSrAlF_6$	oP72	45.3
$CsAgAlF_6$	oP36	48.4
$RbMgAlF_6$	cF72	108.0

Al-Mg systems, as they are expected to disproportionate into the binary hydrides LiH and MgH_2 in the presence of hydrogen and are therefore unlikely to influence the predicted H_2 release reactions. In view of the thermodynamic instability of AlH_3 in the temperature and pressure range of interest for reversible storage,[13] this compound was also excluded from the GCLP input set. The structures of the known compounds are taken from experiments and/or ICSD; since our DFT calculations for these compounds follow standard methodology (see Sec. II), they will not be discussed in detail. The crystal structures of $LiMgAlH_6$ and $LiMg(AlH_4)_3$ have been recently determined using synchrotron x-ray diffraction (XRD) (Refs. 5 and 6) and we report a comprehensive ICSD-based study of the structural stability of $LiMgAlH_6$ below; we have refrained from a similar study for $LiMg(AlH_4)_3$ in view of the thermodynamic instability of the latter. By analogy with the Ca-Al-H system where a stable $CaAlH_5$ compound has been found to exist,[4,18,19] we also investigate the unknown crystal structure and structural stability of a hypothetical $MgAlH_5$ compound.

A. $LiMgAlH_6$

Determination of the crystal structure of $LiMgAlH_6$ has been carried out recently using powder neutron diffraction and synchrotron XRD, resulting in a structure of $P321$ symmetry (prototype $NaCaAlF_6$).[6] Here, we have performed DFT calculations on this and other candidate structures from the inorganic crystal structure database (ICSD) to better understand the energetics and structural properties of $LiMgAlH_6$ and to test the ability of DFT to predict crystal structures of complex hydrides. We used a set of eight trial ICSD structures: α- and β-$NaCaAlF_6$ (mP72 and hP27), $LiCaAlF_6$ (hP18), $LiSrAlF_6$ (hP18), $LiSmAlF_6$ (hP18), $NaSrAlF_6$ (oP72), $CsAgAlF_6$ (oP36), and $RbMgAlF_6$ (cF72). After performing DFT relaxations of atomic positions and cell vectors for all these trial structures, we found that the experimentally observed β-$NaCaAlF_6$ (hP27) structure[6] had the lowest energy (see Table II), providing a good test of the accuracy of the DFT calculations in this system. The next-lowest structures are those of $LiCaAlF_6$ and $LiSrAlF_6$ and that of α-$NaCaAlF_6$, which are all only 7.7 kJ/mol higher in energy than the structure of β-$NaCaAlF_6$, leaving open the possibility that some of these crystal structures may be stabilized by vibrational entropy at high temperatures. The crystal structure of $LiMgAlH_6$ shown in Fig. 1 exhibits hexagonal close packing of hydrogen ions with Al, Mg, and Li ions centered within octahedral cages. Table III summarizes the calculated lattice vectors and ionic coordinates. We find Li-H bond lengths ranging from ~1.86 to ~2.00 Å, Mg-H bond lengths from 1.92 to 1.98 Å, and Al-H bond lengths of ~1.74 Å. Our calculated H-M-H (with M=Li, Mg, Al) bond angles indicate that the LiH_6 octahedra are highly distorted with angles ranging between ~75° and ~103° (Fig. 1), while the AlH_6 cages are nearly ideal, with H-Al-H angles ranging from ~86° to ~91°. Finally, the MgH_6 octahedra exhibit H-Mg-H bond angles between ~84° and ~94°. These findings are in very good agreement with experimental measurements on this compound.[6]

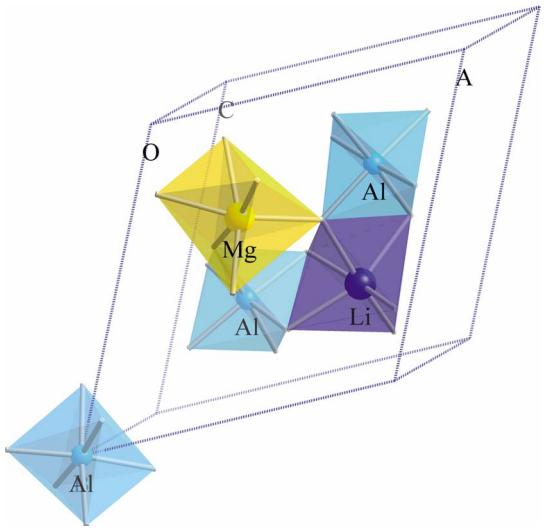

FIG. 1. (Color online) Crystal structure of $LiMgAlH_6$. Li, Mg, and Al octahedra share hydrogen ions, which are at the vertices of these octahedra. Note that the octahedra share edges and corners.

B. $MgAlH_5$

In the Ca alanate system, $CaAlH_5$ has been firmly established as a stable decomposition product,[4,18] which suggests the possible existence of an analogous $MgAlH_5$ compound in

TABLE III. Optimized relaxed atomic coordinates as predicted from first-principles DFT for $LiMgAlH_6$, space group $P32_1$ (No. 150). The calculated DFT lattice parameters are a=7.986 Å, c=4.379 Å, $\alpha=\beta=90°$, and $\gamma=120°$.

Atom	Wyckoff position	x	y	z
Li	3f	0.2954	0	1/2
Mg	3e	−0.3630	0	0
Al1	1a	0	0	0
Al2	2d	1/3	2/3	−0.4976
H1	6g	0.2089	0.1150	0.2200
H2	6g	−0.1268	0.4185	0.2709
H3	6g	−0.4596	−0.2226	0.2772

the closely related Mg alanate system. To the best of our knowledge, $MgAlH_5$ has not yet been observed experimentally, but the structure of this hypothetical compound has been predicted by Klaveness *et al.*[20] using first-principles DFT calculations. Here, we report the results of an extensive ICSD database search using 44 candidate structures with *ANX* type ABX_5 and chemical formula ABC_5, where C=H or F. The structures we use for the ABX_5 stoichiometry include $BaGaF_5$, $BaCrF_5$, $BaAlF_5$, $BaMnF_5$, $CaAlF_5$, $SrVF_5$, $CaFeF_5$, $CdMnF_5$, $CaMnF_5$, $MnCrF_5$, $CaTiF_5$, $CaCrF_5$, $MnAlF_5$, $BaSbF_5$, $KTeF_5$, $SrSbF_5$, $FeAlF_5$, $AuCuF_5$, $CaAlH_5$, $AgBF_5$, $TeKF_5$, $LiUF_5$, $UTlF_5$, $SrAlF_5$, $BaFeF_5$, $SrFeF_5$, $CrMnF_5$, $ULiF_5$, $KZrF_5$, $KTbF_5$, $NaTeF_5$, $TbKF_5$, $ZrKF_5$, $TeNaF_5$, $TeTlF_5$, $CsTbF_5$, $CuAuF_5$, $TeCsF_5$, $SRbF_5$, $TeRbF_5$, $RbTeF_5$, $RbSF_5$, $CsTeF_5$, and $TbCsF_5$. Some of these chemical compositions appear more than once in ICSD, corresponding to different structural polymorphs, which exist at different temperature and pressure conditions. These prototype structures are enumerated in Table IV with the corresponding Pearson symbols and the total energies relative to the lowest-energy structure found in this study—the orthorhombic $P2_12_12_1$ structure (space group No. 19, prototype $BaGaF_5$). In all cases, full structural relaxations of atomic positions and lattice vectors were carried out according to the initial symmetry of the ICSD structure. Several of the ICSD prototype structures had identical energies and symmetries, and only the distinct ones are given in Table IV. We find that the $BaGaF_5$-type structure is 7.8 kJ/mol lower in energy than the $CaFeF_5$ prototype, in qualitative disagreement with the theoretical predictions of Ref. 20, which placed the $BaGaF_5$-type structure above $CaFeF_5$. The relative energies of three candidate structures with lowest energies ($BaGaF_5$-, $CaFeF_5$-, and $BaMnF_5$-type) were essentially unchanged for every combination of pseudopotentials and gradient-corrected exchange-correlation functionals supplied in the standard VASP pseudopotential package (we tried both PW91[9] and Perdew-Burke-Erzenhoff[21]). Furthermore, our relaxed atomic positions and lattice constants for $CaFeF_5$-type $MgAlH_5$ are very similar to those given in Ref. 20. Since the calculated energy differences between the $CaFeF_5$ and $BaGaF_5$ structures are well above the numerical uncertainties due to the size of the basis set, the choice of the ionic pseudopotentials or density of the **k**-point mesh, the reasons for the discrepancy with the results of Ref. 20 are presently unclear. Table V shows the optimized relaxed atomic coordinates for the lowest-energy $P2_12_12_1$ structure predicted in this study and Fig. 2 shows the crystal structure of $MgAlH_5$. We find that Al-H bond lengths range between 1.64 and 1.81 Å, and the Al-H-Al bond angles range from ~83° to ~96°, indicating that the corner-sharing AlH_6 octahedra comprising the crystal structure of $MgAlH_5$ are slightly distorted.

TABLE IV. ABC_5 prototype structures and relative DFT energetics w.r.t. lowest-energy prototype structure, i.e., $BaGaF_5$, obtained in the DFT database searching for the ground state of $MgAlH_5$. Only the results for 32 distinct structures are shown here.

ABC_5 prototype	Pearson symbol	Energy (kJ/mol)
BaGaF5	oP28	0
BaMnF5	oP28	7.4
CaAlF5	mS28	7.7
SrVF5	mP56	7.8
CaFeF5	mP28	7.8
CdMnF5	mC14	8.0
CaMnF5	mS28	8.0
MnAlF5	oC14	11.2
BaSbF5	oP28	11.3
FeAlF5	oI7	12.4
AuCuF5	aP7	13.0
CaAlH5	mP56	17.2
AgBF5	tP14	22.6
TeKF5	oP28	22.9
LiUF5	tI112	25.4
UTlF5	mP56	28.7
SrAlF5	tI56	29.4
BaFeF5	tI112	29.5
SrFeF5	mP56	35.8
CrMnF5	mS28	36.7
ULiF5	tI56	39.9
KZrF5	aP42	43.6
NaTeF5	oP28	45.8
TbKF5	aP42	52.1
TeNaF5	oP28	54.9
TeTlF5	oP28	58.5
CsTbF5	oS56	78.6
CuAuF5	aP7	83.2
TeCsF5	oP28	89.0
TeRbF5	oP56	108.5
RbSF5	oP28	112.7
TbCsF5	oC28	262.3

IV. THERMODYNAMICS AND DECOMPOSITION PATHWAYS

A. Vibrational effects on thermodynamics

Table I summarizes the calculated formation enthalpies ΔH_f, zero-point energies (ZPEs), vibrational energies, and reaction entropies at T=300 K for all the metal hydrides and Li-Mg alanates considered in this paper. The formation energies are given with respect to gaseous H_2 and elemental bulk metals (fcc Al, fcc Li, and hcp Mg). All compounds except $Mg(AlH_4)_2$ (see below) are found to be dynamically stable, and our DFT calculations are in good agreement with other theoretical studies, as well as with the available experimental data.

To test the accuracy of the calculated thermodynamic properties, we examined the convergence of the vibrational enthalpy and entropy with respect to the size of the supercell for Al, MgH_2, $LiMgAlH_6$, and $Mg(AlH_4)_2$. The results are presented in Table VI, showing that zero-point energies and vibrational enthalpies $H_{\mathrm{vib}}^{300\ \mathrm{K}}$ are converged within

TABLE V. Optimized relaxed atomic coordinates as predicted from first-principles DFT for $MgAlH_5$, with space group $P2_12_12_1$ (No. 19), and the lattice parameters of a=4.550 Å, b=4.260 c =13.024 Å, and $\alpha=\beta=\gamma=90°$.

Atom	Wyckoff position	x	y	z
Mg	4a	−0.2504	−0.2466	−0.3204
Al	4a	0.2486	0.2528	−0.4083
H1	4a	−0.4756	−0.0559	0.4069
H2	4a	−0.0300	0.0912	0.3051
H3	4a	0.4719	−0.0516	−0.4063
H4	4a	0.0284	0.0975	−0.3045
H5	4a	−0.0024	0.0916	−0.4994

~1 kJ/mol, while the vibrational entropies are converged to better than 5 J/mol K for our choice of supercells. In the case of $Mg(AlH_4)_2$, using a $2\times2\times2$ supercell with 8 f.u., we find several slightly unstable phonon modes involving zone-boundary optical vibrations of AlH_4 tetrahedra. Separate energy-versus-displacement calculations following the unstable mode eigenvectors confirm the instabilities, revealing the presence of symmetrically placed minima at energies less than 0.05 kJ/mol below the $P\bar{3}m_1$ structure. Due to the weakness of these instabilities, it is likely that they will become anharmonically stabilized at high temperatures. We circumvent the practical difficulties of calculating the vibrational

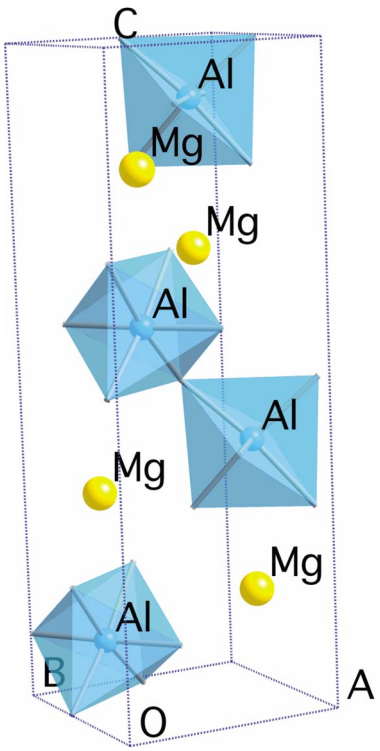

FIG. 2. (Color online) The predicted lowest-energy crystal structure of $MgAlH_5$ ($BaGaF_5$ prototype, space group $P2_12_12_1$, Pearson symbol oP28). Mg ions are yellow, Al (blue) ions are in the center of corner-sharing octahedra, and H ions are at the vertices of these octahedra.

TABLE VI. Convergence of the calculated ZPE, vibrational energies $H_{vib}^{300\ K}$, and vibrational entropies $S_{vib}^{300\ K}$ with respect to the supercell size for Al, MgH_2, $LiMgAlH_6$, and $Mg(AlH_4)_2$.

Number of atoms	ZPE (kJ/mol)	$H_{vib}^{300\ K}$ (kJ/mol)	$S_{vib}^{300\ K}$ (J/mol K)
	Al		
8	3.2	7.1	25.4
27	3.6	7.9	26.2
64	3.6	8.0	27.0
	MgH_2		
48	39.08	44.6	32.7
72	39.00	44.3	30.1
216	39.10	44.6	31.9
	$LiMgAlH_6$		
27	125.5	138.7	72.4
54	126.6	140.5	77.3
	$Mg(AlH_4)_2$		
11	146.8	167.2	126.8
88	154.4	178.3	152.7

entropies of harmonically unstable $P\bar{3}m_1$ by performing full structural relaxations starting from the positions of the energy minima for the unstable modes. We find that a structure with the space group $P\bar{3}$ (No. 147) with 4 f.u. per unit cell is 0.2 kJ/mol lower in energy than $P\bar{3}m_1$ and has stable phonons.[22] The results in Table VI show that the vibrational entropy of $Mg(AlH_4)_2$ is increased by 26 J/mol K when going from a $1\times1\times1$ to $2\times2\times2$ supercell, demonstrating the importance of using sufficiently large supercells for obtaining accurate entropies. However, it is difficult to estimate the uncertainty in the calculated entropy value for $Mg(AlH_4)_2$ due to the approximate treatment of the entropy contributions from the unstable modes.

Table VII lists the calculated reaction enthalpies and entropies in the Li-Mg-Al-H system, with and without the vibrational contributions to the reaction thermodynamics. Our calculations confirm that zero-point vibrational contributions typically lower the dehydrogenation enthalpies by as much as 15 kJ/(mol H_2), which is in agreement with previous studies on other complex hydrides (see, for instance, Ref. 14 and references therein). This effect can be explained by the existence of rotational, H-Al-H bond-bending, and Al-H bond-stretching modes in alanates and by the lack of corresponding translational and rotational ZPE contributions for H_2 molecules; these factors combine to lower the vibrational energy balance in the dehydrogenated state. Inclusion of the finite-temperature vibrational energies and enthalpy of H_2 gas (given by $\frac{7}{2}k_BT$) acts to increase the calculated T =300 K enthalpies relative to their T=0 K, ZPE values. In all cases, the T=300 K dehydrogenation enthalpies with vibrational effects are lower than the static values obtained

TABLE VII. Reaction thermodynamics in the Li-Mg-Al-H system. ΔH^{static} is the static DFT enthalpy at $T=0$ K without the ZPE contributions, $\Delta H^{0\ \text{K}}$ is the $T=0$ K enthalpy with ZPE, $\Delta H^{300\ \text{K}}$ is the $T=300$ K enthalpy including the vibrational energies and the enthalpy of H_2 gas, and $\Delta S^{300\ \text{K}}$ is the reaction entropy at $T=300$ K. For compound formation reactions without H_2 release (reactions 1–4), enthalpies are given in units of kJ/mol, while for hydrogen release reactions (5–12) enthalpies are given in units of kJ/(mol H_2). Reaction entropies are given in units of J/mol K for reactions 1–4 and in J/(mol H_2 K) for reactions 5–12. The reaction enthalpies calculated by other authors ("other DFT") or measured experimentally ("Exp") are also given for comparison.

No.	Reaction	ΔH^{Static}	$\Delta H^{0\ \text{K}}$	$\Delta H^{300\ \text{K}}$	$\Delta H^{\text{Other DFT}}$	ΔH^{Exp}	$\Delta S^{300\ \text{K}}$
	Formation of mixed alanate compounds						
	$LiMg(AlH_4)_3$						
1	$LiAlH_4+Mg(AlH_4)_2\rightarrow LiMg(AlH_4)_3$	−9.3	−6.8	−8.8			−17.0
	$LiMgAlH_6$						
2	$1/3\,Li_3AlH_6+1/3\,Mg(AlH_4)_2+2/3\,MgH_2\rightarrow LiMgAlH_6$	−23.9	−18.3	−21.4			−25.5
3	$LiAlH_4+MgH_2\rightarrow LiMgAlH_6$	−19.6	−12.8	−16.4			−25.7
4	$1/3\,Li_3AlH_6+2/3\,MgAlH_5+1/3\,MgH_2\rightarrow LiMgAlH_6$	−16.4	−14.6	−15.5			−5.6
	Hydrogen release reactions						
	$LiMg(AlH_4)_3$						
5	$LiMg(AlH_4)_3\rightarrow LiMgAlH_6+2Al+3H_2$	−3.6	−12.3	−7.3		−5.0[a] (427 K)	+104.6
	$LiMgAlH_6$						
6	$LiMgAlH_6\rightarrow LiH+MgH_2+Al+1.5H_2$	+25.6	+10.3	+18.6		+8.7[a] (458 K)	+130.7
7	$LiMgAlH_6\rightarrow 1/3\,Li_3AlH_6+MgH_2+2/3\,Al+H_2$	+23.7	+7.7	+16.6			+133.0
	Li alanates						
8	$3LiAlH_4\rightarrow Li_3AlH_6+2Al+3H_2$	+4.1	−5.1	+0.2	+9.8[b]	+3.5[b] (298 K)	+106.1
9	$Li_3AlH_6\rightarrow 3LiH+Al+1.5H_2$	+29.6	+15.4	+22.8	+31.4[b]	+28.9[b] (298 K)	+125.9
	Mg alanates						
10	$Mg(AlH_4)_2\rightarrow MgH_2+2Al+3H_2$	−0.23	−10.4	−4.8		−0.57[a] (458 K)	+107.5
11	$Mg(AlH_4)_2\rightarrow MgAlH_5+Al+1.5H_2$	−7.7	−13.7	−10.8			+87.7
12	$MgAlH_5\rightarrow MgH_2+Al+1.5H_2$	+7.3	−6.9	+1.1			+127.4

[a]Reference 4.
[b]Reference 27.

without vibrations. The magnitude of this enthalpy lowering effect at $T=300$ K is not large for Li-Mg alanates—it typically constitutes 5 kJ/(mol H_2) and is never higher than 10 kJ/(mol H_2), in agreement with the conclusions of Ref. 23. Interestingly, Table VII shows that the calculated entropy of hydrogen release varies within a rather wide range between approximately 90 and 150 J/(mol H_2 K). We find that in all cases where reaction entropies are significantly lower than the standard state entropy of H_2 gas [$\Delta S^0=130.68$ J/(K mol H_2) at $T=20\ ^\circ$C and $p=1$ bar (Ref. 24)], the corresponding H_2 release reactions involve transformations from tetrahedrally bonded $[AlH_4]^{3-}$ to octahedrally bonded $[AlH_6]^{3-}$ complexes (see reactions 5, 8, and 11 in Table VII). As previously noted in Ref. 16, entropy lowering can be explained by counting the number of low-frequency rotational and translational modes in the compounds on the

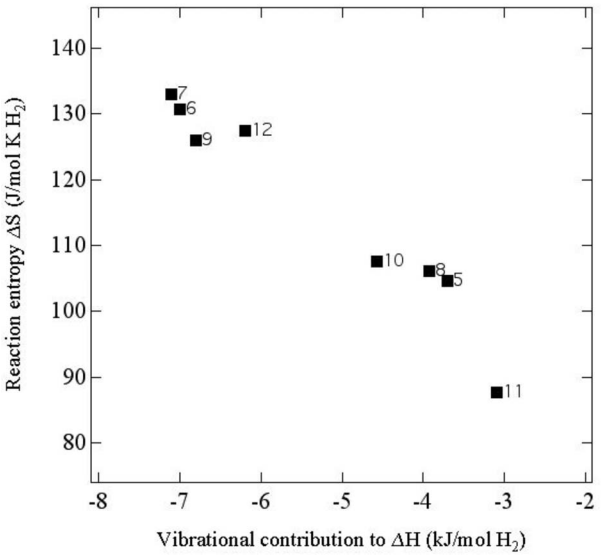

FIG. 3. $T=300$ K reaction entropies versus vibrational contributions to the reaction enthalpies for all hydrogen release reactions in Table VII.

right and left sides of the hydrogen release reaction. Indeed, each metal cation gives rise to three translational branches, while each complex anion generates three translational and three rotational branches, resulting in six low-frequency branches (H-Al-H bond-bending and Al-H bond-stretching modes have much higher energies and do not contribute to the entropy at ambient temperatures). Taking reaction 5 from Table VII as an example, $LiMg(AlH_4)_3 \rightarrow LiMgAlH_6+2Al+3H_2$, there are two cations and three AlH_4 complex anions on the left-hand side, resulting in $2\times3+3\times6=24$ low-frequency phonon branches in $LiMg(AlH_4)_3$. On the right-hand side of reaction 5, $LiMgAlH_6$ has $2\times3+6=12$ low-frequency translational and rotational modes, with another six translational modes coming from 2 f.u. of bulk Al, giving a total of 18 low-frequency modes. Since the ambient-temperature entropy of complex hydrides is dominated by the translational and rotational modes, simple mode counting properly accounts for the loss of vibrational entropy when going from the reactants to the products. This simple physical picture is quite general and has been shown to apply to other complex hydrides with anions such as $[BH_4]^-$ and $[B_{12}H_{12}]^{2-}$.[16]

Figure 3 indicates that the reaction *entropy* anticorrelates with the vibrational contributions to the reaction *enthalpies*. This is somewhat surprising, since at the temperature ranges of interest the enthalpies and entropies are determined by different parts of the vibrational spectra: while the entropies are dominated by the low-frequency phonons, the reaction enthalpies contain sizable contributions from zero-point vibrations and are given by a sum over the whole frequency range, including the stiff internal vibrations of the complex anions. The observed anticorrelation between ΔH_{vib} and ΔS suggests that the zero-point energies of high-frequency internal modes might be comparable in all compounds containing the same type of complex anion (e.g., for all alanates), and the relative variation in vibrational enthalpies between different reactions is explained by the low-frequency part of the phonon spectrum, just like for reaction entropies. Loss of low-frequency phonon modes in the product phases relative to the reactants will then result in a decrease in the reaction entropies and increase in $T>0$ K reaction enthalpies, in accord with the data presented in Fig. 3.

B. Mixed alanates: $LiMg(AlH_4)_3$ and $LiMgAlH_6$

Reaction 1 in Table VII shows that the calculated formation enthalpy of $LiMg(AlH_4)_3$ is negative at 300 K indicating stability with respect to phase separation into lithium and magnesium alanates. The vibrational contribution to the formation entropy of $LiMg(AlH_4)_3$ at 300 K is also found to be negative, and the overall free energy of formation $\Delta G=\Delta H-T\Delta S$ is extremely small in magnitude but negative (-1.7 kJ/mol). Therefore, our calculations predict that the mixed tetra-alanate is marginally stable with respect to decomposition into $LiAlH_4$ and $Mg(AlH_4)_2$. The calculated free energy is at the limit of the numerical and physical accuracy of our calculations, and we show below that the compound is actually unstable with respect to H_2 release at ambient conditions. In contrast, the formation of the mixed hexa-alanate $LiMgAlH_6$ is strongly exothermic (see reactions 2–4 in Table VII).

Another interesting result seen from Table VII concerns the formation enthalpy of $LiMg(AlH_4)_3$ and $LiMgAlH_6$ via reactions 1–3, which shows that the contribution of zero-point vibrations to the formation enthalpies may be quite large (~7 kJ/mol) even for reactions that do not involve hydrogen release. A convenient way to rationalize these surprising results is by considering the atom-decomposed ZPE contributions to the formation enthalpies, which are given in Table VIII. These data show that most of the ZPE contribution to the enthalpies of reactions 1–3 comes from the hydrogen ions, indicating that the vibrational frequencies of hydrogen vary substantially with the bonding topology even within the same multinary system. The calculated phonon spectra are shown in Fig. 4, which shows the partial atom-decomposed and total PDOSs for $LiMg(AlH_4)_3$ and $LiMgAlH_6$. We find that the phonon modes of $LiMg(AlH_4)_3$ and $LiMgAlH_6$ are grouped in three distinct frequency regions: (i) low-frequency vibrations of Li, Mg, and Al ions below 50 meV, (ii) intermediate frequency regions corresponding to H-Al-H, Mg-H-Mg, and Li-H-Li bond-bending modes between 50 and 125 meV for $LiMg(AlH_4)_3$, and between 50 and 150 meV for $LiMgAlH_6$, and (iii) high-frequency regions with Al-H bond-stretching modes above 200 meV for $LiMg(AlH_4)_3$, and above 150 meV for $LiMgAlH_6$. Even though the general features of the phonon spectra are similar to what we calculated for pure Li and Mg alanates (these data are not shown here), subtle shifts in the peak positions are responsible for the sizable vibrational contributions to the calculated formation enthalpies of the mixed alanates.

Using the linear programming approach of Ref. 14, we have verified that $LiMgAlH_6$ is thermodynamically stable with respect to phase separation into all possible combinations of known compounds in the Li-Mg-Al-H system. Fur-

TABLE VIII. Atom-decomposed ZPE contributions to the formation enthalpies of reactions 1–4 from Table VII (in kJ/mol).

Reaction	ΔH_{vib} (H)	ΔH_{vib} (Li)	ΔH_{vib} (Mg)	ΔH_{vib} (Al)	Total
1	+3.03	−0.29	−0.10	−0.13	+2.51
2	+5.26	+0.04	−0.22	+0.54	+5.62
3	+5.48	+0.67	−0.31	+0.98	+6.82
4	+1.54	+0.31	−0.09	+0.04	+1.80

thermore, from the linear programming approach, we also find that $LiMg(AlH_4)_3$ is thermodynamically unstable and decomposes exothermically via reaction 5 into $LiMgAlH_6$, Al, and H_2. Our calculations predict very weak exothermic enthalpies of −7.3 and −6.9 kJ/(mol H_2) at $T=300$ and 430 K, respectively, which compare very well with the experimentally measured weak exothermic enthalpy at 427 K [−5.0 kJ/(mol H_2)].[4] Therefore, we conclude that $LiMg(AlH_4)_3$ is not useful for reversible on-board storage because of poor thermodynamics and associated instability toward H_2 release. The mixed hexahydride $LiMgAlH_6$ has two thermodynamically competitive endothermic decomposition pathways given by reactions 6 and 7 in Table VII. One of these pathways (reaction 6) leads directly to the formation of binary hydrides LiH and MgH_2 and metallic Al, while the other (reaction 7) proceeds via an intermediate step involving Li_3AlH_6 and MgH_2. The calculated $T=300$ K reaction enthalpies and entropies of both of these pathways are very close, which is a consequence of the fact that the decomposition thermodynamics of Li_3AlH_6 (reaction 9) are very similar to those of $LiMgAlH_6$ via reactions 6 and 7. It will be very difficult, if not impossible, to distinguish these reactions experimentally because their enthalpies are nearly equal and hydrogen release usually occurs only at above-equilibrium temperatures, where none of the hexahydrides are stable. Our calculations yield $T=460$ K reaction enthalpies of +21.2 and +19.2 kJ/(mol H_2) for reactions 6 and 7, respectively. In qualitative agreement with our results, the differential scanning calorimetry (DSC) measurements of Ref. 4 for the decomposition reaction 6 indicate an endothermic peak at 458 K, with a reaction enthalpy of +8.7 kJ/(mol H_2). Further investigations are needed to clarify the source for the numerical discrepancy between our calculations and DSC results. We note that the GGA is known to *underestimate* the formation enthalpy of MgH_2 by as much as 15 kJ/mol.[25,26] Since reactions 6 and 7 involve the formation of MgH_2 as a reaction product, underestimating the stability of the right-hand side of these reactions may contribute to the calculated dehydrogenation enthalpies, which are higher than the experimentally measured values.

C. Lithium alanate

Reactions 8 and 9 constitute the well-known two-step decomposition for $LiAlH_4$. In the first step, $LiAlH_4$ decomposes into Li_3AlH_6 and Al according to reaction 8. This step has a weakly endothermic reaction enthalpy of +0.2 kJ/mol H_2 at 300 K, which agrees well with the experimentally measured value of +3.5 kJ/(mol H_2),[27] but is somewhat different from an earlier DFT value of +9.8 kJ/(mol H_2) calculated in Ref. 27. In the second step, Li_3AlH_6 decomposes into LiH and Al via the endothermic reaction 9 with a calculated $T=300$ K DFT enthalpy of +22.8 kJ/(mol H_2), which is slightly lower than the experimentally measured value of +28.9 kJ/(mol H_2), but higher than an earlier DFT value of 15.7 kJ/(mol H_2) obtained in Ref. 27. Although the calculated reaction enthalpy falls within the target range for reversible hydrogen storage (20–50 kJ/mol H_2), the kinetics and reversibility of this reaction would need to be improved for practical use.

D. Magnesium alanates: $Mg(AlH_4)_2$ and $MgAlH_5$

Magnesium alanate $Mg(AlH_4)_2$ has been experimentally determined to decompose exothermically into MgH_2, Al, and H_2 (Ref. 4) according to reaction 10 from Table VII. Our calculated reaction enthalpy is also slightly exothermic, −4.8 kJ/(mol H_2) at 300 K, which is in good agreement with the experimentally measured value of −0.57 kJ/(mol H_2) at 458 K (Ref. 4) and prior first-principles calculations.[28] Our DFT results confirm that $Mg(AlH_4)_2$ is not useful for reversible hydrogen storage because it is too unstable thermodynamically and therefore cannot be easily rehydrogenated. Recently, there have been studies on the chemically similar Ca alanate system, where $Ca(AlH_4)_2$ was also found to be thermodynamically unstable at ambient conditions, decomposing exothermically into a stable $CaAlH_5$ compound, Al, and H_2.[4,18,19] Here, we investigate whether $MgAlH_5$ is a stable intermediate compound in the decomposition sequence of Mg alanate. Reactions 11 and 12 represent a hypothetical two-step decomposition pathway. We find that static DFT energetics (excluding ZPE) predict that reaction 11, forming $MgAlH_5$, has an exothermic reaction enthalpy of −7.7 kJ/(mol H_2), while the second step (decomposition of $MgAlH_5$ into MgH_2, Al, and H_2) has an endothermic enthalpy of +7.3 kJ/(mol H_2). Therefore, *static* DFT energetics appear to predict that $MgAlH_5$ is a thermodynamically stable intermediate compound in the decomposition sequence of $Mg(AlH_4)_2$ at sufficiently low temperatures and/or high H_2 pressures. However, including ZPE contributions changes these conclusions qualitatively. It is seen from the data in Table VII that upon including ZPE, both reactions 11 and 12 become exothermic already at $T=0$ K, demonstrating that very high H_2 pressures would be necessary to stabilize these compounds thermodynamically. At $T=300$ K, the enthalpy of decomposition of $MgAlH_5$ be-

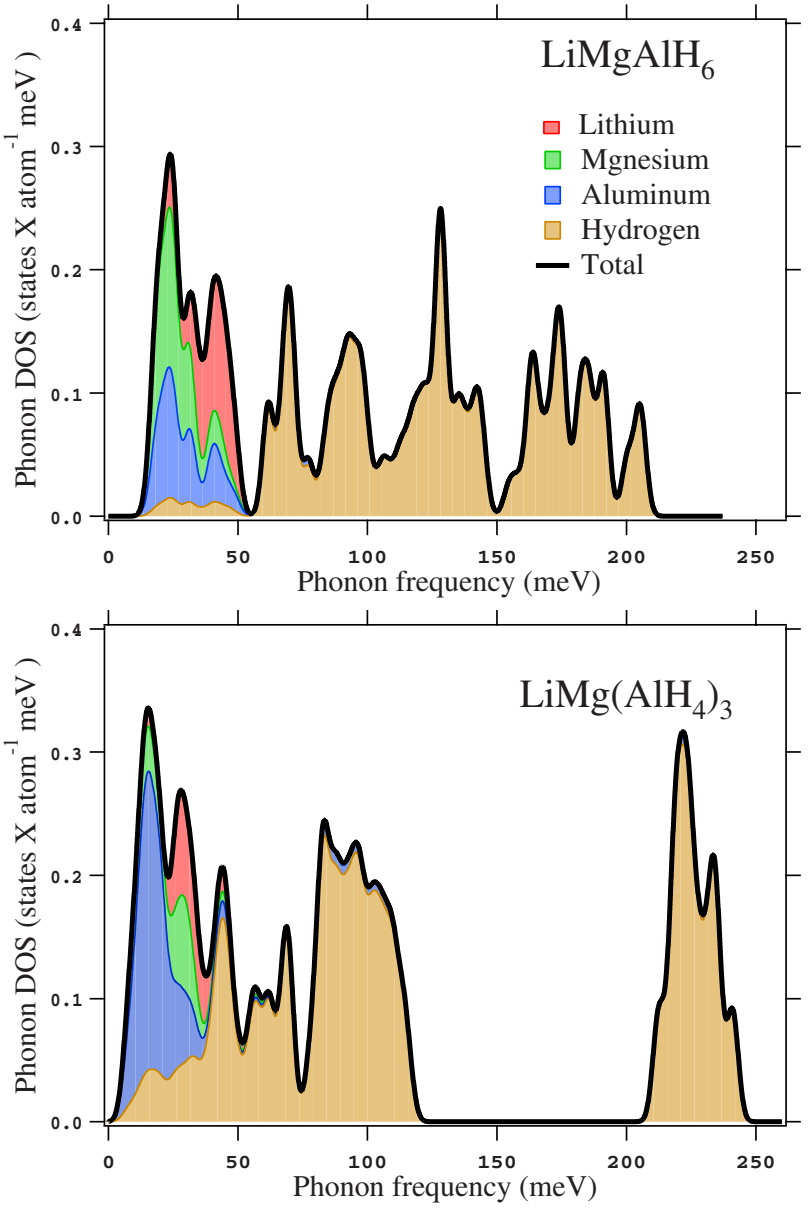

FIG. 4. (Color online) The calculated phonon densities of states for $LiMgAlH_6$ and $LiMg(AlH_4)_3$. The red, green, blue, and orange, represent Li, Mg, Al, and H partial contributions to DOS, respectively, and the solid lines indicate the total DOS.

comes slightly endothermic (+1.1 kJ/mol H_2), however the compound is still unstable thermodynamically under practically useful H_2 pressures. We conclude that the formation of $MgAlH_5$ is highly unlikely to occur during a typical room-temperature decomposition experiment, even though it might be possible to form $MgAlH_5$ directly using a solid-state ion-exchange reaction or a solution-phase synthesis route.

V. CONCLUSIONS

Using the first-principles DFT approach in conjunction with database searching, we have confirmed the crystal structure of $LiMgAlH_6$ and predicted the crystal structure of $MgAlH_5$. For the former, we find that the lowest-energy structure is that of the prototype $NaCaAlF_6$ compound with the space group $P321$, in agreement with recent experimental data, confirming the accuracy and efficiency of database searching for predicting crystal structures of unknown metal hydride structures. For $MgAlH_5$, our first-principles calculations indicate that $BaGaF_5$-type structure is the lowest-energy ground state. Our results also indicate that vibrational free-energy contributions destabilize $MgAlH_5$ at ambient H_2 pressures and that both $Mg(AlH_4)_2$ and $MgAlH_5$ are not useful for reversible storage since they are thermodynamically unstable. Phonon contributions to the reaction enthalpies have been determined for all compounds in the Li-Mg-Al-H system. In agreement with previous studies, the zero-point vibrational energies lower the calculated $T=0$ K reaction enthalpies by 10–20 kJ/(mol H_2) relative to the static DFT values without vibrations. However, the full inclusion of room-temperature vibrational enthalpies and the enthalpy of H_2 gas leads to a more modest lowering of the reaction en-

thalpy by less than 10 kJ/(mol H_2). Interestingly, we also find that the enthalpies of the formation reactions of mixed Li-Mg alanates, reactions 1–3 in Table VII, are significantly affected by the vibrational enthalpies, even though no hydrogen gas is released in these reactions. Reaction entropies for all hydrogen release reactions involving the transformation from $[AlH_4]^-$ to $[AlH_6]^{3-}$ complex anions are found to be significantly below the standard state entropy of H_2 gas, which we explain by the decrease in the number of low-frequency translational and rotational phonon branches in the dehydrogenated reaction products relative to the hydrogen-rich reactants.

ACKNOWLEDGMENTS

A.A. and V.O. gratefully acknowledge financial support from the U.S. Department of Energy under Grant No. DE-FG02-05ER46253. C.W. was supported by the National Science Foundation under Grant No. CBET-0730929.

[1] F. Schüth, B. Bogdanović, and M. Felderhoff, Chem. Commun. (Issue 20), 2249 (2004).
[2] B. Bogdanović and M. Schwickardi, J. Alloys Compd. **253-254**, 1 (1997).
[3] J. Graetz and J. J. Reilly, Scr. Mater. **56**, 835 (2007).
[4] M. Mamatha, B. Bogdanović, M. Felderhoff, A. Pommerin, W. Schmidt, F. Schüth, and C. Weidenthaler, J. Alloys Compd. **407**, 78 (2006).
[5] H. Grove, H. W. Brinks, R. H. Heyn, F.-J. Wu, S. M. Opalka, X. Tang, B. L. Laube, and B. C. Hauback, J. Alloys Compd. **455**, 249 (2007).
[6] H. Grove, H. W. Brinks, Ole M. Løvvik, R. H. Heyn, and B. C. Hauback, J. Alloys Compd. **460**, 64 (2007).
[7] O. M. Løvvik and O. Swang, Europhys. Lett. **67**, 607 (2004); M. H. Sørby, H. W. Brinks, A. Fossdal, K. Thorshaug, and B. C. Hauback, J. Alloys Compd. **415**, 284 (2006).
[8] O. M. Løvvik, O. Swang, and S. M. Opalka, J. Mater. Res. **20**, 3199 (2005).
[9] J. P. Perdew and Y. Wang, Phys. Rev. B **45**, 13244 (1992).
[10] P. E. Blöchl, Phys. Rev. B **50**, 17953 (1994).
[11] G. Kresse and J. Furthmüller, Phys. Rev. B **54**, 11169 (1996); G. Kresse and J. Furthmüller, Comput. Mater. Sci. **6**, 15 (1996); G. Kresse and J. Hafner, Phys. Rev. B **47**, 558 (1993); G. Kresse and J. Hafner, J. Phys.: Condens. Matter **6**, 8245 (1994); G. Kresse and J. Hafner, Phys. Rev. B **49**, 14251 (1994); G. Kresse and D. Joubert, *ibid.* **59**, 1758 (1999).
[12] H. J. Monkhorst and J. D. Pack, Phys. Rev. B **13**, 5188 (1976).
[13] C. Wolverton, V. Ozolins, and M. Asta, Phys. Rev. B **69**, 144109 (2004).
[14] A. R. Akbarzadeh, V. Ozoliņš, and C. Wolverton, Adv. Mater. (Weinheim, Ger.) **19**, 3233 (2007).
[15] E. H. Majzoub and V. Ozolins, Phys. Rev. B **77**, 104115 (2008); V. Ozolins, E. H. Majzoub, and C. Wolverton, Phys. Rev. Lett. **100**, 135501 (2008).
[16] V. Ozoliņš, E. H. Majzoub, and C. Wolverton, J. Am. Chem. Soc. **131**, 230 (2009).
[17] Sudhakar V. Alapati, J. Karl Johnson, and David S. Sholl, J. Phys. Chem. C **112**, 5258 (2008).
[18] C. Weidenthaler, T. J. Frankcombe, and M. Felderhoff, Inorg. Chem. **45**, 3849 (2006).
[19] C. Wolverton and V. Ozolins, Phys. Rev. B **75**, 064101 (2007).
[20] A. Klaveness, P. Vajeeston, P. Ravindran, H. Fjellvåg, and A. Kjekshus, Phys. Rev. B **73**, 094122 (2006).
[21] J. P. Perdew, K. Burke, and M. Ernzerhof, Phys. Rev. Lett. **77**, 3865 (1996).
[22] See EPAPS Document No. E-PRBMDO-79-058914 for the online supplementary information. For more information on EPAPS, see http://www.aip.org/pubservs/epaps.html
[23] S. V. Alapati, J. K. Johnson, and D. S. Sholl, J. Phys. Chem. C **111**, 1584 (2007).
[24] M. W. Chase, C. A. Davies, J. R. Downey, D. J. Frurip, R. A. McDonald, and A. N. Syverud, J. Phys. Chem. Ref. Data Suppl. **14**, (Suppl. 1) (1985).
[25] B. Bogdanović, A. Ritter, and B. Spliethoff, Angew. Chem. Int. Ed. Engl. **29**, 223 (1990); L. G. Hector, J. F. Herbst, W. Wolf, P. Saxe, and G. Kresse, Phys. Rev. B **76**, 014121 (2007); M. Pozzo and D. Alfè, *ibid.* **77**, 104103 (2008); J. J. Vajo, F. Mertens, C. C. Alm, R. C. Bowman, and B. Fultz, J. Phys. Chem. B **108**, 13977 (2004).
[26] J. F. Stampfer, C. E. Holley, and J. F. Suttle, J. Am. Chem. Soc. **82**, 3504 (1960).
[27] O. M. Løvvik, S. M. Opalka, H. W. Brinks, and B. C. Hauback, Phys. Rev. B **69**, 134117 (2004).
[28] M. J. van Setten, G. A. de Wijs, V. A. Popa, and G. Brocks, Phys. Rev. B **72**, 073107 (2005).
[29] N. Sklar and B. Post, Inorg. Chem. **6**, 669 (1967).
[30] T. N. Dymova, D. P. Aleksandrov, V. N. Konoplev, T. A. Silina, and A. S. Sizareva, Russ. J. Coord. Chem. **20**, 279 (1994).
[31] P. Claudy, B. Bonnetot, J. M. Letoffe, and G. Turck, Thermochim. Acta **27**, 213 (1978).
[32] Sai-Cheong Chung and H. Morioka, J. Alloys Compd. **372**, 92 (2004).
[33] M. Fichtner, J. Engel, O. Fuhr, A. Gloss, O. Rubner, and R. Ahlrichs, Inorg. Chem. **42**, 7060 (2003).